15 Nuclear Methods

15.1 General Remarks

Several nuclear methods are important for diffusion studies in solids. They are listed in Table 13.1 and their potentials are illustrated in Fig. 13.1. The first of these methods is nuclear magnetic resonance or nuclear magnetic relaxation (NMR). NMR methods are mainly appropriate for self-diffusion measurements on solid or liquid metals. In favourable cases self-diffusion coefficients between about 10^{-20} and $10^{-10}\,\mathrm{m^2\,s^{-1}}$ are accessible. In the case of foreign atom diffusion, NMR studies suffer from the fact that a signal from nuclear spins of the minority component must be detected.

Mössbauer spectroscopy (MBS) and quasielastic neutron scattering (QENS) are techniques, which have considerable potential for understanding diffusion processes on a microscopic level. The linewidths $\Delta\Gamma$ in MBS and in QENS have contributions which are due to the diffusive motion of atoms. This diffusion broadening is observed only in systems with fairly high diffusivities since $\Delta\Gamma$ must be comparable with or larger than the natural linewidth in MBS experiments or with the energy resolution of the neutron spectrometer in QENS experiments. Usually, the workhorse of MBS is the isotope ^{57}Fe although there are a few other, less favourable Mössbauer isotopes such as ^{119}Sn,^{115}Eu, and ^{161}Dy. QENS experiments are suitable for fast diffusing elements with a large incoherent scattering cross section for neutrons. Examples are Na self-diffusion in sodium metal, Na diffusion in ion-conducting rotor phases, and hydrogen diffusion in metals.

Neither MBS nor QENS are routine methods for diffusion measurements. The most interesting aspect is that these methods can provide *microscopic information* about the elementary jump process of atoms. The linewidth for single crystals depends on the atomic jump frequency and on the crystal orientation. This orientation dependence allows the deduction of the *jump direction* and the *jump length* of atoms, information which is not accessible to conventional diffusion studies.

15.2 Nuclear Magnetic Relaxation (NMR)

The technique of nuclear magnetic relaxation has been widely used for many years to give detailed information about condensed matter, especially about

its atomic and electronic structure. It was recognised in 1948 by Bloembergen, Purcell and Pound [1] that NMR measurements can provide information on diffusion through the influence of atomic movement on the width of nuclear resonance lines and on relaxation times. Atomic diffusion causes fluctuations of the local fields, which arise from the interaction of nuclear magnetic moments with their local environment. The fluctuating fields either can be due to magnetic dipole interactions of the magnetic moments or due to the interaction of nuclear electric quadrupole moments (for nuclei with spins $I > 1/2$) with internal electrical field gradients. In addition, external magnetic field gradients can be used for a direct determination of diffusion coefficients.

We consider below some basic principles of NMR. Our prime aim is an understanding of how diffusion influences NMR. Solid state NMR is a very broad field. For a comprehensive treatment the reader is referred to textbooks of Abragam [2], Slichter[3], Mehring [4] and to chapters in monographs and textbooks [5–9]. In addition, detailed descriptions of NMR relaxation techniques are available, e.g., in [10]). Corresponding pulse programs are nowadays implemented in commercial NMR spectrometers.

15.2.1 Fundamentals of NMR

NMR methods are applicable to atoms with non-vanishing nuclear spin moment, $\hbar I$, and an associated magnetic moment

$$\mu = \gamma \hbar I \,, \tag{15.1}$$

where γ is the gyromagnetic ratio, I the nuclear spin, and $\hbar$ the Planck constant divided by 2π. In a static magnetic field $\boldsymbol{B_0}$ in z-direction, a nuclear magnetic moment $\boldsymbol{\mu}$ performs a precession motion around the z-axis governed by the equation

$$\frac{\mathrm{d}\boldsymbol{\mu}}{\mathrm{d}t} = \boldsymbol{\mu} \otimes \boldsymbol{B_0} \,. \tag{15.2}$$

The precession frequency is the Larmor frequency

$$\omega_0 = \gamma B_0. \tag{15.3}$$

The degeneracy of the $2I+1$ energy levels is raised due to the nuclear Zeeman effect. The energies of the nuclear magnetic dipoles are quantised according to

$$U_m = -m\gamma\hbar B_0 \,, \tag{15.4}$$

where the allowed values correspond to $m = -I, -I+1, \ldots, I-1, I$. For example, for nuclei with $I = 1/2$ there are only two energy levels with the energy difference $\hbar\omega_0$.

At thermal equilibrium, the spins are distributed according to the Boltzmann statistics on the various levels. Since the energy difference between

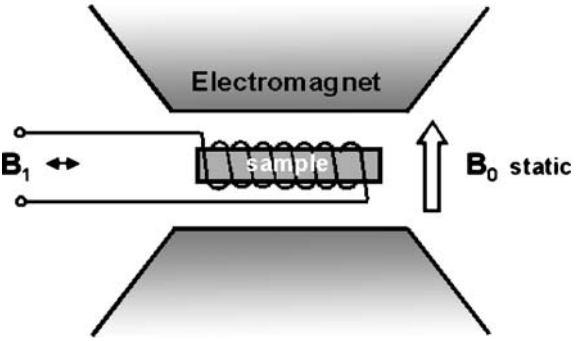

Fig. 15.1. Set-up for a NMR experiment (schematic)

levels for typical magnetic fields (0.1 to 1 Tesla) is very small, the population difference of the levels is also small. A macroscopic sample in a static magnetic field $\boldsymbol{B}_0$ in the z-direction displays a magnetisation $\boldsymbol{M}^{eq}$ along the z-direction and a transverse magnetisation $M_\perp = 0$. The equilibrium magnetisation of an ensemble of nuclei (number density N) is given by

$$\boldsymbol{M}^{eq} = N\frac{\gamma^2\hbar^2 I(I+1)}{3k_{\mathrm{B}}T}\boldsymbol{B}_0\,. \tag{15.5}$$

A typical experimental set-up for NMR experiments (Fig. 15.1) consists of a sample placed in a strong, homogeneous magnetic field $\boldsymbol{B}_0$ of the order of a few Tesla. A coil wound around the sample permits the application of an alternating magnetic field $\boldsymbol{B}_1$ perpendicular to the z-direction with frequency ω. Typically, these fields are radio-frequency (r.f.) fields. If the frequency ω of the transverse r.f. field $\boldsymbol{B}_1$ is close to the Larmor frequency, this field will induce transitions between the Zeeman levels of the nuclear spins. In NMR-spectrometers the coil around the sample is used for several steps of the experiment, such as irradiation of r.f. pulses and detection of the free induction decay of the ensemble of nuclei (see below).

The analysis of NMR experiments proceeds via a consideration of detailed interactions among nuclear moments and between them and other components of the solid such as electrons, point defects, and paramagnetic impurities. This theory has been developed over the past decades and can be found, e.g., in the textbooks of Abragam [2] and Slichter [3]. Although this demands the use of quantum mechanics, much can be represented by semi-classical equations proposed originally by Bloch. The effect of rf-pulse sequences on the time evolution of the total magnetisation $\boldsymbol{M}$ in an external field

$$\boldsymbol{B} = \boldsymbol{B}_0 + \boldsymbol{B}_1 \tag{15.6}$$

is given by the Bloch equation [2, 3]:

$$\frac{\mathrm{d}\boldsymbol{M}}{\mathrm{d}t} = \gamma \boldsymbol{M} \otimes \boldsymbol{B} - \frac{M_\perp}{T_2} - \frac{M_z - M_z^{eq}}{T_1} + \nabla \left[D \nabla (\boldsymbol{M} - \boldsymbol{M}^{eq}) \right] . \qquad (15.7)$$

The first term in Eq. (15.7) describes the precession of the spins around the magnetic field $\boldsymbol{B}$. The second and third terms give the rate of relaxation of the magnetisation and define two phenomenological constants, T_1 and T_2, denoted as relaxation times. They pertain to the longitudinal and transverse components of the magnetisation. In the absence of any transverse field, T_1 determines the rate at which M_z returns to its equilibrium value M_z^{eq}. This relaxation corresponds to an energy transfer between the spin-system and the so-called 'lattice', where the 'lattice' represents all degrees of freedom of the material with the exception of those of the spin-system. Therefore, T_1 is denoted as the *spin-lattice relaxation time*. T_2 refers to the transverse part of the nuclear magnetisation and is called the *spin-spin relaxation time*. Nuclear spins can be brought to a state of quasi-thermal equilibrium among themselves without being in thermal equilibrium with the lattice. T_2 describes relaxation to such a state. It follows that $T_2 \leq T_1$. T_2 is closely related to the width of the NMR signal.

The last term in Eq. (15.7) was introduced by Torrey [11] and describes the time evolution of the magnetisation $\boldsymbol{M}$, when the sample is also put into a magnetic field gradient. $\boldsymbol{M}^{eq}$ is the equilibrium value of the magnetic moment in field B_0 and D the diffusion coefficient. Equation (15.7) shows that various NMR techniques can be used to deduce information about atomic diffusion.

Elegant pulse techniques of radiofrequency spectroscopy permit the direct determination of D and of the relaxation times T_1 and T_2 (see, e.g., Gerstein and Dybowski [10]).

15.2.2 Direct Diffusion Measurement by Field-Gradient NMR

When a sample is placed deliberately in a magnetic field gradient, $G = \partial B/\partial z$, in addition to a static magnetic field, a direct determination of diffusion coefficients is possible. The basis of such NMR experiments in an inhomogeneous magnetic field is the last term of the Bloch equation. In a magnetic field gradient the Larmor frequency of a nuclear moment depends on its positions. Field-gradient NMR (FG-NMR) utilises the fact that nuclear spins that diffuse in a magnetic field-gradient experience an irreversible phase shift, which leads to a decrease in transversal magnetisation. This decay can be observed in so-called spin-echo experiments [12, 13]. The amplitude of the spin-echo is given by

$$M_G(t_{echo}) = M_0(t_{echo}) \exp \left[-\gamma^2 D \int_0^{t_{echo}} \left(\int_0^{t'} G(t'') \, \mathrm{d}t'' \right)^2 \mathrm{d}t' \right] , \qquad (15.8)$$

where

$$M_0(t_{echo}) \;=\; M_0(0)\exp\left(-\frac{t_{echo}}{T_2}\right) . \tag{15.9}$$

t_{echo} denotes the time of the spin echo. $M_G(t_{echo})$ and $M_0(t_{echo})$ are the echo amplitudes with and without field-gradient $G(t)$. $M_0(0)$ is the equilibrium magnetisation of the spin system.

For a 90-τ-180-τ spin-echo pulse sequence we have $t_{echo} = 2\tau$. In a constant magnetic field gradient G_0 the solution of Eq. (15.8) is proportional to the transversal magnetisation $M_\perp$, which is given by

$$M_G(2\tau) = M_0(0)\exp\left(-\frac{2\tau}{T_2}\right)\exp\left(-\frac{2}{3}\gamma^2 D G_0^2 \tau^3\right) . \tag{15.10}$$

By varying τ or G_0 the diffusion coefficient can be determined from the measured spin-echo amplitude. The diffusion of spins is followed directly by FG-NMR. Thus, FG-NMR is comparable to tracer diffusion. For a known G_0 value a measurement of the diffusion-related part of the spin echo *versus* time can provide the diffusion coefficient without any further hypothesis. In contrast to tracer diffusion, the FG-NMR technique permits diffusion measurements in isotopically pure systems.

Equation (15.10) shows that the FG-NMR technique is applicable when the spin-spin relaxation time T_2 of the sample is large enough. A significant diffusion-related decay of the spin-echo amplitude must occur within T_2. For fixed values of T_2 and G_0 this requires D-values that are large enough. The measurement of small D-values requires high field-gradients. This can be achieved by using pulsed magnetic field-gradients (PFG) as suggested by McCall [14]. The first experiments with PFG-NMR were performed by Stejskal and Tanner [13] for diffusion studies in aqueous solutions. For a comprehensive review of PFG-NMR spectroscopy the reader is referred, for example, to the reviews of Stilbs [15], Kärger et al. [16], and Majer [7]. PFG-NMR has been widely applied to study diffusion of hydrogen in metals and intermetallic compounds [7]. Applications to anomalous diffusion processes such as diffusion in porous materials and polymeric matrices can be found in [16]. Diffusion of hydrogen in solids is a relatively fast process and the proton is particularly suited for NMR studies due to its high gyromagnetic ratio. Diffusivities of hydrogen between 10^{-10} and 10^{-13} have been studied by PFG-NMR [7].

A fine example for the application of PFG-NMR are measurements of self-diffusion of liquid lithium and sodium [17]. Figure 15.2 displays self-diffusivities in liquid and solid Li obtained by PFG-NMR according to Feinauer and Majer [18]. At the melting point, the diffusivity in liquid Li is almost three orders of magnitude faster than in the solid state. Also visible is the isotope effect of Li diffusion. The diffusivity of ^{6}Li is slightly faster than that of ^{7}Li.

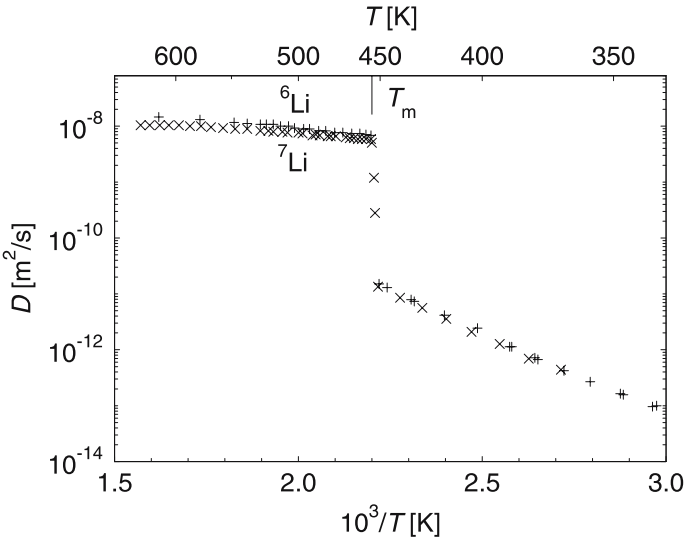

Fig. 15.2. Self-diffusion of ^{6}Li and ^{7}Li in liquid and solid Li studied by PFG-NMR according to Feinauer and Majer [18]

15.2.3 NMR Relaxation Methods

Indirect NMR methods for diffusion studies measure either the relaxation times T_1 and T_2, or the linewidth of the absorption line. In addition, other relaxation times not contained in the Bloch equation can be operationally defined. The best known of these is the spin-lattice relaxation time in the rotating frame, $T_{1\rho}$. This relaxation time characterises the decay of the magnetisation when it is 'locked' parallel to B_1 in a frame of reference rotating around B_0 with the Larmor frequency $\omega_0 = \gamma B_0$. In such an experiment, $\boldsymbol{M}$ starts from $\boldsymbol{M}^{eq}$ and decays to $B_1 M^{eq}/B_0$. Since $T_{1\rho}$ is shorter than T_1, measurements of $T_{1\rho}$ permit the detection of slower atomic motion than T_1.

Let us consider a measurement of the spin-lattice relaxation time T_1. If a magnetic field is applied in the z-direction, T_1 describes the evolution of the magnetisation M_z towards equilibrium according to

$$\frac{\mathrm{d}M_z}{\mathrm{d}t} = \frac{M_z^{eq} - M_z}{T_1} \,. \tag{15.11}$$

A measurement of T_1 proceeds in two steps. (i) At first, the nuclear magnetisation is inverted by the application of an 'inversion pulse'. (ii) Then, the magnetisation $M_z(t)$ is observed by a 'detection pulse' as it relaxes back to the equilibrium magnetisation.

The effect of r.f. pulses can be discussed on the basis of the Bloch equation (15.7). If the resonance condition, $\omega_0 = \gamma B_0$, is fulfilled for the alternating $\boldsymbol{B}_1$ field, the magnetisation will precess in the y-z plane with a precession

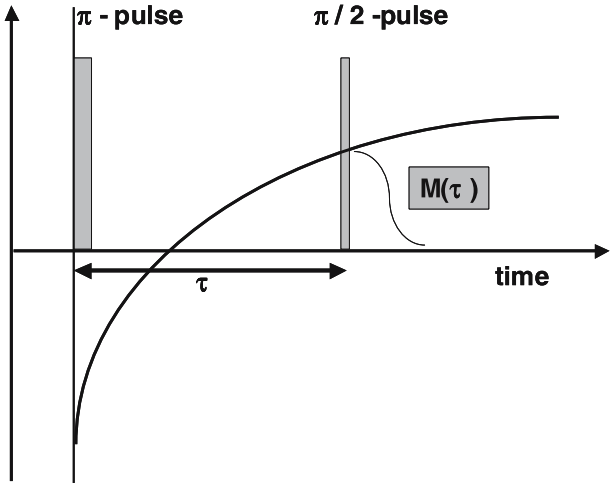

Fig. 15.3. Schematic iluustration of a T_1 measurement with an inversion-recovery (π-τ-$\pi/2$) pulse sequence

frequency γB_1. The application of a pulse of the r.f. field B_1 with a duration t_p will result in the precession of the magnetisation to the angle $\Theta_p = \gamma B_1 t_p$. By suitable choice of the pulse length the magnetisation can be inverted ($\Theta_p = \pi$) or tilted into the x-y plane ($\Theta_p = \pi/2$). During precession in the x-y plane the magnetisation will induce a voltage in the coil (Fig. 15.1). This signal is called the *free induction decay* (FID). If, for example, an initial π-pulse is applied, $M_z(t)$ can be monitored by the amplitude of FID after a $\pi/2$-reading pulse at the evolution time t, which is varied in the experiment[1]. This widely used pulse sequence for the measurement of T_1 is illustrated in Fig. 15.3.

NMR is sensitive to interactions of nuclear moments with fields produced by their local environment. The relaxation times and the linewidth are determined by the interaction between nuclear moments either directly or via electrons. Apart from coupling to the spins of conduction electrons in metals or of paramagnetic impurities in non-metals, two basic mechanisms of interaction must be considered in relation to atomic movements. The first interaction is dipole-dipole coupling among the nuclear magnetic moments. The second interaction is due to nuclear electric quadrupole moments with internal electric field gradients. Nonzero quadrupolar moments are present for nuclei with nuclear spins $I > 1/2$. The diffusion of nuclear moments causes variations in both of these interactions. Therefore, the width of the resonance line and the relaxation times have contributions which are due to the thermally activated jumps of atoms.

[1] Without discussing further details, we mention that more complex pulse sequences have been tailored to overcome limitations of the simple sequence, which suffers from the dead-time of the detection system after the strong r.f. pulse.

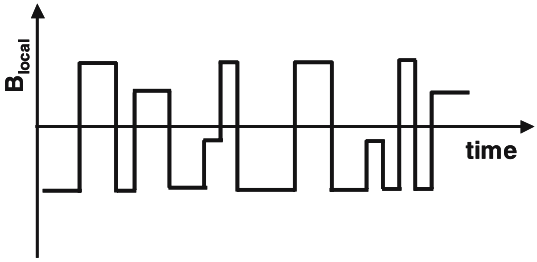

Fig. 15.4. Temporal fluctuations of the local field – the origin of motional narrowing

Spin-Spin Relaxation and Motional Narrowing: Let us suppose for the moment that we need to consider only magnetic dipole interactions, which is indeed the case for nuclei with $I = 1/2$. Each nuclear spin precesses, in fact, in a magnetic field $\boldsymbol{B} = \boldsymbol{B}_0 + \boldsymbol{B}_{local}$, where $\boldsymbol{B}_{local}$ is the local field created by the magnetic moments of neighbouring nuclei. The local field experienced by a particular nucleus is dominated by the dipole fields created by the nuclei in its immediate neighbourhood, because dipolar fields vary as $1/r^3$ with the distance r between the nuclei. Since the nuclear moments are randomly oriented, the local field varies from one nucleus to another. This leads to a dispersion of the Larmor frequency and to a broadening of the resonance line according to

$$\Delta\omega_0 \; = \; \frac{1}{T_2} \; \propto \gamma \Delta B_{local} \, . \tag{15.12}$$

ΔB_{local} is an average of the local fields in the sample. In solids without internal motion, local fields are often quite large and give rise to rather short T_2 values. Typical values without motion of the nuclei are the following: $\Delta B_{local} \approx 2 \times 10^{-4}$ Tesla, $T_2 \approx 100 \mu$s and $\Delta\omega_0 \approx 10^4$ rad s^{-1}. Such values are characteristic of a 'rigid lattice' regime. The pertaining spin-spin relaxation time is denoted as T_2 (*rigid lattice*).

Let us now consider how diffusion affects the spin-spin relaxation time and the linewidth of the resonance line. Diffusion comes about by jumps of individual atoms from one site to another. The mean residence time of an atom, $\bar{\tau}$, is temperature dependent via

$$\bar{\tau} = \tau_0 \exp\left(\frac{\Delta H}{k_{\mathrm{B}} T}\right) \tag{15.13}$$

with an activation enthalpy ΔH and a pre-factor τ_0. Each time when an atom jumps into a new site, its nuclear moment will find itself in another local field. As a consequence, the local field sensed by a nucleus will fluctuate between $\pm B_{local}$ on a time-scale characterised by the mean residence time (Fig. 15.4). If the mean residence time of an atom is much shorter than the spin-spin relaxation time of the rigid lattice, i.e. for $\bar{\tau} \ll T_2$ (*rigid lattice*),

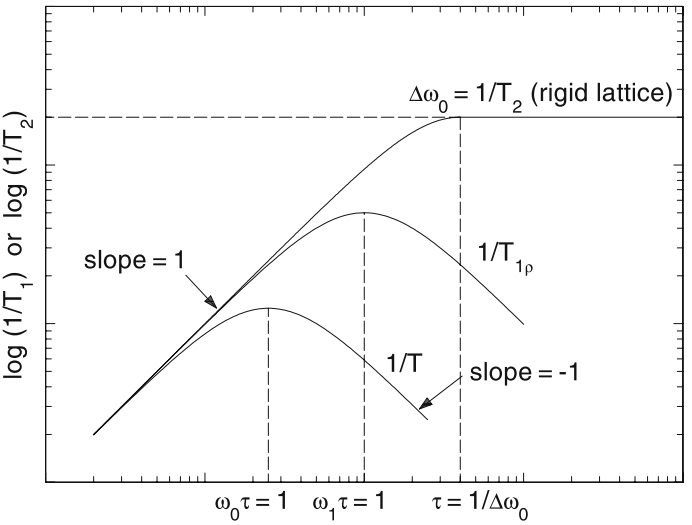

Fig. 15.5. Schematic illustration of diffusional contributions (random jumps) to spin-lattice relaxation rates, $1/T_1$ and $1/T_{1\rho}$, and to the spin-spin relaxation rate $1/T_2$

a nuclear moment will sample many different local fields. The nuclear moment will behave as though it were in some new effective local field, which is given by the average of all the local fields sampled. If the sampled local fields vary randomly in direction and magnitude this average will be quite small, depending on how many are sampled. The dephasing between the spins grows more slowly with time than in a fixed local field. The effective local fields of all the nuclear moments will be small, and the nuclear moments will precess at nearly the same frequency. Thus, the nuclear moments will not lose their coherence as rapidly during a FID, and T_2 will be longer. A longer FID is equivalent to a narrower resonance line.

If the diffusion rate is increased, it can be shown by statistical considerations that the width of the resonance line becomes

$$\Delta\omega' = \frac{1}{T_2'} = \Delta\omega_0^2 \bar{\tau}\,. \tag{15.14}$$

This phenomenon is called *motional narrowing*. A schematic illustration of the temperature dependence the spin-spin relaxation rate $1/T_2$ is displayed in Fig. 15.5: at low temperatures the relaxation rate of the rigid lattice is observed, since diffusion is so slow that an atom does not even jump once during the FID; as $\bar{\tau}$ gets shorter with increasing temperature $1/T_2'$ decreases and the width of the resonance line gets narrower.

Spin-Lattice Relaxation: When discussing the Bloch equations we have seen that the spin-lattice relaxation time T_1 is the characteristic time during

which the nuclear magnetisation returns to its equilibrium value. We could also say the nuclear spin system comes to equilibrium with its environment, called 'lattice'. In contrast to spin-spin relaxation, this process requires an exchange of energy with the 'lattice'. Spin-lattice relaxation either takes place by the absorption or emission of phonons or by coupling of the spins to conduction electrons (via hyperfine interaction) in metals. The relaxation rate due to the coupling of nuclear spins with conduction electrons is approximately given by the Koringa relation

$$\left(\frac{1}{T_1}\right)_e = \text{const} \times T, \tag{15.15}$$

where T denotes the absolute temperature. The relaxation rate due to dipolar interactions, $(1/T_1)_{dip}$, and due to quadrupolar interactions, $(1/T_1)_Q$, is added to that of electrons, so that the total spin-lattice relaxation rate is

$$\frac{1}{T_1} = \left(\frac{1}{T_1}\right)_e + \left(\frac{1}{T_1}\right)_{dip} + \left(\frac{1}{T_1}\right)_Q . \tag{15.16}$$

For systems with nuclear spins $I = 1/2$, quadrupolar contributions are absent.

The fluctuating fields can be described by a correlation function $G(t)$, which contains the temporal information about the atomic diffusion process [2, 3]. Let us assume as in the original paper by Bloembergen, Purcell and Pound [1] that the correlation function decays exponentially with the correlation time τ_c, i.e. as

$$G(t) = G(0) \exp\left(-\frac{|\,t\,|}{\tau_c}\right) . \tag{15.17}$$

This behaviour is characteristic of jump diffusion in a three dimensional system and τ_c is closely related to the mean residence time between successive jumps. The Fourier transform of Eq. (15.17), which is called the *spectral density function* $J(\omega)$, is a Lorentzian given by

$$J(\omega) = G(0)\frac{2\tau_c}{1+\omega^2\tau_c^2} . \tag{15.18}$$

Transitions between the energy levels of the spin-system can be induced, i.e. spin-lattice relaxation becomes effective, when $J(\omega)$ has components at the transition frequency. The spin-lattice relaxation rate is then approximately given by

$$\left(\frac{1}{T_1}\right)_{dip} \approx \frac{3}{2}\gamma^4\hbar^2 I(I+1)J(\omega_0) . \tag{15.19}$$

Detailed expressions for the relaxation rates $\frac{1}{T_1}$, $\frac{1}{T_2}$ and $\frac{1}{T_{1\rho}}$ can be found, e.g., in [2, 6].

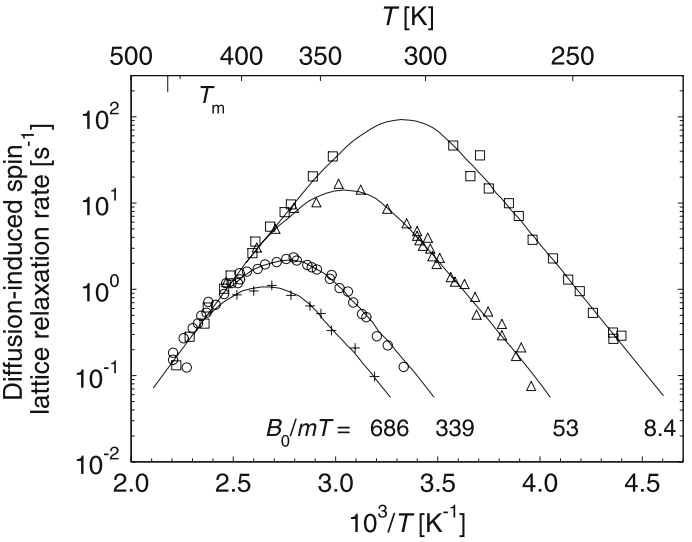

Fig. 15.6. Diffusion-induced spin-lattice relaxation rate, $(1/T_1)_{dip}$, of ^{8}Li in solid Li as a function of temperature according to HEITJANS ET AL. [8]. The B_0 values correspond to Larmor frequencies $\omega_0/2\pi$ of 4.32 MHz, 2.14 MHz, 334 kHz, and 53 kHz

The correlation time τ_c, like the mean residence time $\bar{\tau}$, will usually obey an Arrhenius relation

$$\tau_c = \tau_c^0 \exp\left(\frac{\Delta H}{k_\mathrm{B} T}\right) , \tag{15.20}$$

where ΔH is the activation enthalpy of the diffusion process. Since the movement of either atom of a pair will change the correlation function we may identify τ_c with one half of the mean residence time $\bar{\tau}$ of an atom at a lattice site.

The diffusion-induced spin-lattice relaxation rate, $(1/T_1)_{dip}$, is shown in Fig. 15.6 for self-diffusion of ^{8}Li in lithium according to HEITJANS ET AL. [8]. In a representation of the logarithm of the relaxation rate as function of the reciprocal temperature, a symmetric peak is observed with a maximum at $\omega_0\tau_c \approx 1$. At temperatures well above or below the maximum, which correspond to the cases $\omega_0\tau_c \ll 1$ or $\omega_0\tau_c \gg 1$, the slopes yield $\Delta H/k_\mathrm{B}$ or $-\Delta H/k_\mathrm{B}$.

The work of BLOEMBERGEN, PURCELL AND POUND [1] is based on the assumption of the exponential correlation function of Eq. (15.17), which is appropriate for diffusion in liquids. Later on, the theory was extended to random walk diffusion in lattices by TORREY [19]. Based on the *encounter model* (see Chap. 7) the influence of defect mechanisms of diffusion and the associated correlation effects have been included into the theory by WOLF [20] and MACGILLIVRAY AND SHOLL [21]. These refinements lead to results that

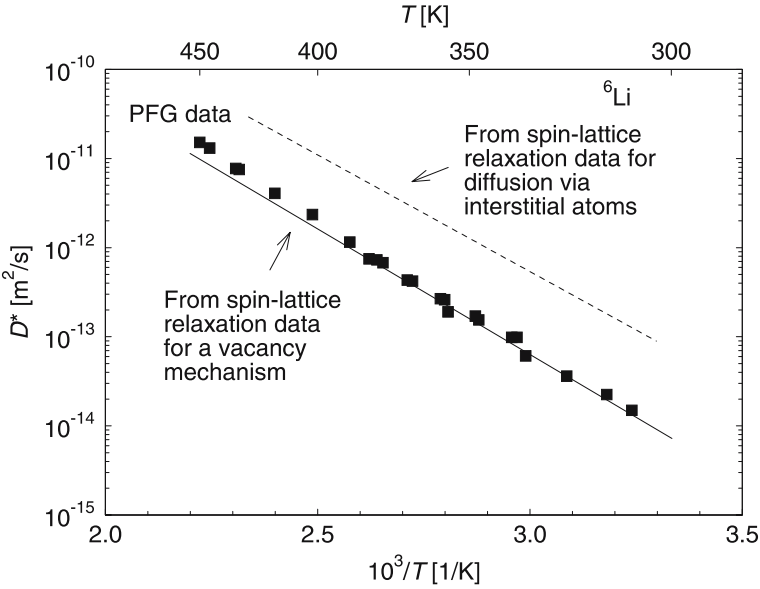

Fig. 15.7. Comparison of self-diffusivities for ^{6}Li in solid Li determined by PFG-NMR with spin-lattice relaxation results assuming a vacancy mechanism (*solid line*) and an interstitial mechanism (*dashed line*) according to MAJER [22]

are broadly similar to those of [1]. However, the refinements are relevant for a quantitative interpretation of NMR results in terms of diffusion coefficients. We illustrate this by an example:

Figure 15.7 shows a comparison of diffusion data of ^{6}Li in solid lithium obtained with PFG-NMR and data deduced from relaxation measurements. PFG-NMR yields directly ^{6}Li self-diffusion coefficients in solid lithium. No assumption about the elementary diffusion steps is needed for these data. The dashed and solid lines are deduced from $(1/T_1)_{dip}$ data, assuming two different atomic mechanisms. Good coincidence of diffusivities from spin-lattice relaxation and the PFG-NMR data is obtained with the assumption that Li diffusion is mediated by vacancies. Direct interstitial diffusion clearly can be excluded [22].

15.3 Mössbauer Spectroscopy (MBS)

The Mössbauer effect has been detected by the 1961 Nobel laureate in physics R. MÖSSBAUER [23]. The Mössbauer effect is the recoil-free emission and absorption of γ-radiation by atomic nuclei. Among many other applications, Mössbauer spectroscopy can be used to deduce information about the movements of atoms for which suitable Mössbauer isotopes exist. There are only

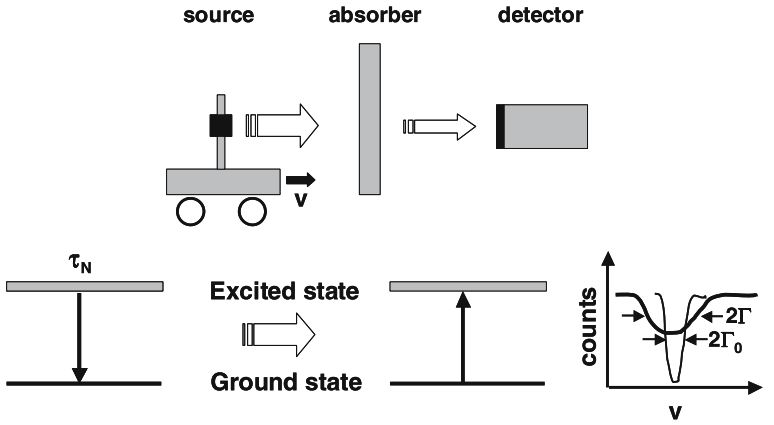

Fig. 15.8. Mössbauer spectroscopy. *Top*: moving source experiment; *bottom*: principles

a few nuclei, ^{57}Fe, ^{119}Sn, ^{151}Eu, and ^{161}Dy, for which Mössbauer spectroscopy can be used. ^{57}Fe is the major 'workhorse' of this technique

Information about atomic motion is obtained from the broadening of the otherwise very narrow γ-line. Thermally activated diffusion of Mössbauer atoms contributes to the linewidth in a way first recognised by SINGWI AND SJÖLANDER in 1960 [24] soon after the detection of the Mössbauer effect.

Mössbauer spectroscopy uses two samples, one playing the rôle of the source, the other one the rôle of an absorber of γ-radiation as indicated in Fig. 15.8. In the source the nuclei emit γ-rays, some of which are absorbed without atomic recoil in the absorber. The radioisotope ^{57}Co is frequently used in the source. It decays with a half-life time of 271 days into an excited state of the Mössbauer isotope ^{57}Fe. The Mössbauer level is an excited level of ^{57}Fe with lifetime $\tau_N = 98$ ns. It decays by emission of γ-radiation of the energy $E_\gamma = 14.4\,\mathrm{keV}$ to the ground state of ^{57}Fe, which is a stable isotope with a 2.2% natural abundance. If the Mössbauer isotope is incorporated in a crystal, the recoil energy of the decay is transferred to the whole crystal. Then, the width of the emitted γ-line becomes extremely narrow. This is the effect for which Mössbauer received the Nobel price. The absorber also contains the Mössbauer isotope. A fraction f of the emitted γ-rays is absorbed without atomic recoil in the absorber. In the experiment, the source is usually moved relative to the absorber with a velocity v. Experimantal set-ups with static source and a moving absorber are also possible. This motion causes a Doppler shift

$$\Delta E = \frac{v}{c} E_\gamma \tag{15.21}$$

of the source radiation, where c denotes the velocity of light. The linewidth in the absorber is then recorded as a function of the relative velocity or as a function of the Doppler shift ΔE.

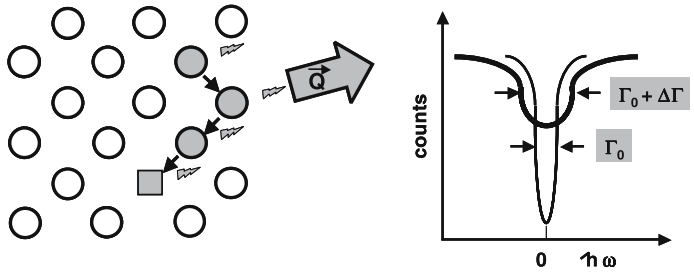

Fig. 15.9. Simplified, semi-classical explanation of the diffusional line-broadening of a Mössbauer spectrum. $\boldsymbol{Q}$ denotes the wave vector of the γ-rays

Diffusion in a solid, if fast enough, leads to a diffusional broadening of the Mössbauer spectrum. This can be understood in a simplified picture as illustrated in Fig. 15.9 [25]: at low temperatures, the Mössbauer nuclei stay on their lattice sites during the emission process. Without diffusion the natural linewidth Γ_0 is observed, which is related to the lifetime of the excited Mössbauer level, τ_N, via the Heisenberg uncertainty relation:

$$\Gamma_0 \tau_N \geq \hbar \,. \tag{15.22}$$

At elevated temperatures, the atoms become mobile. A diffusing atom resides on one lattice site only for a time $\bar{\tau}$ between two successive jumps. If $\bar{\tau}$ is of the same order or smaller than τ_N, the Mössbauer atom changes its position during the emission process. When an atom is jumping the wave packet emitted by the atom is 'cut' into several shorter wave packets. This leads to a broadening of the linewidth Γ, in addition to its natural width Γ_o. If $\bar{\tau} \ll \tau_N$, the broadening, $\Delta\Gamma = \Gamma - \Gamma_0$, is of the order of

$$\Delta\Gamma \approx \hbar/\bar{\tau} \,. \tag{15.23}$$

Neglecting correlation effects (see, however, below) and considering diffusion on a Bravais lattice with a jump length d the diffusion coefficient is related to the diffusional broadening via

$$D \approx \frac{d^2}{12} \frac{\Delta\Gamma}{\hbar} \,. \tag{15.24}$$

Experimental examples for Mössbauer spectra of ^{57}Fe in iron are shown in Fig. 15.10 according to Vogl and Petry [27]. The Mössbauer source was ^{57}Co. The linewidth increases with increasing temperature due to the diffusional motion of Fe atoms. Figure 15.11 shows an Arrhenius diagram of self-diffusion for γ- and δ-iron, in which the Mössbauer data are compared with tracer results [27]. The jump length d in Eq. (15.24) was assumed to be the nearest neighbour distance of Fe. It can be seen that

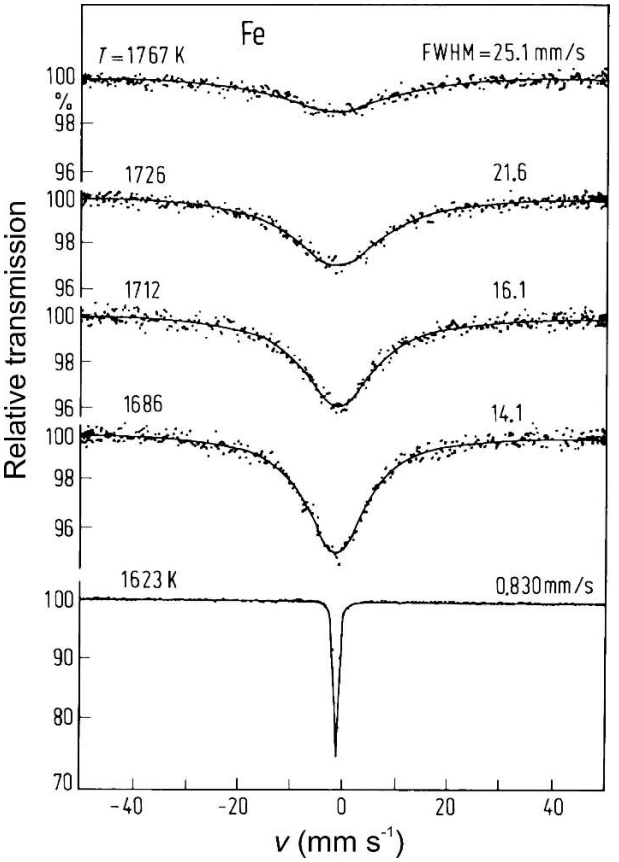

Fig. 15.10. Mössbauer spectra for self-diffusion in polycrystalline Fe from a review of Vogl and Petry [27]. FWHM denotes the full-width of half maximum of the Mössbauer line. The spectrum at 1623 K pertains to γ-iron and the spectra at higher temperatures to δ-iron

the diffusivities determined from the Mössbauer study agree within error bars with diffusivities from tracer studies. Equation (15.24) is an approximation and follows from the more general Eq. (15.27). For this aim Eq. (15.27) is specified to polycrystalline samples and considered for $Q \gg 1/d$. For 14.4 keV γ-radiation we have $Q = 73\ \mathrm{nm}^{-1}$, which is indeed much larger than $1/d$. The broadening is more pronounced in the high-temperature δ-phase of iron with the bcc structure as compared to the fcc γ-phase of iron. This is in accordance with the fact that self-diffusion increases by about one order of magnitude, when γ-iron transforms to δ-iron (see Chap. 17).

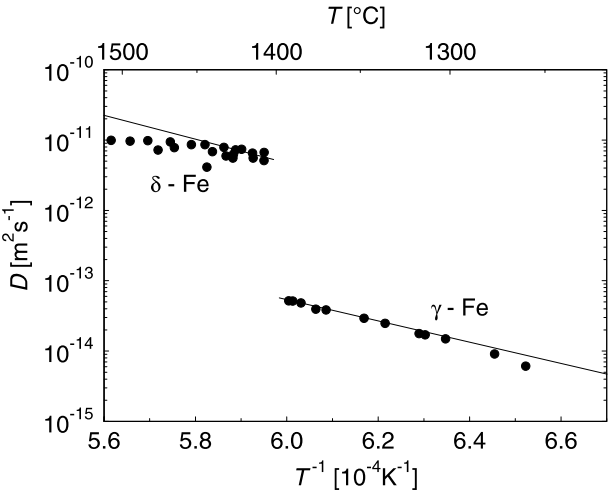

Fig. 15.11. Self-diffusion in γ- and δ-iron: comparison of Mössbauer (*symbols*) and tracer results (*solid lines*) according to VOGL AND PETRY [27]

Diffusional Broadening of MBS Signals: A quantitative analysis of diffusional line-broadening uses the fact that according to VAN HOVE [28] the displacement of atoms in space and time can be described by the self-correlation function $G_s(\boldsymbol{r}, t)$. This is the probability density to find an atom displaced by the vector $\boldsymbol{r}$ within a time interval t. We are interested in the self-correlation function because the Mössbauer absorption spectrum, $\sigma(\boldsymbol{Q}, \omega)$, is related to the double Fourier transform of G_s in space and time via

$$\sigma(\boldsymbol{Q}, \omega) \;\propto\; Re\left[\int\int G_s(\boldsymbol{r}, t) \exp\left[i(\boldsymbol{Q}\cdot\boldsymbol{r} - \omega t) - \Gamma_0 \mid t \mid /2\hbar\right] \mathrm{d}\boldsymbol{r}\mathrm{d}t\right] , \tag{15.25}$$

where Γ_0 is the natural linewidth of the Mössbauer transition.

The self-correlation function contains both diffusional motion as well as lattice vibrations. Usually, these two contributions can be separated. The vibrational part leads to the so-called Debye-Waller factor, f_{DW}, which governs the intensity of the resonantly absorbed radiation. The diffusional part determines the shape of the Mössbauer spectrum. As the wave packets are emitted by the same nucleus, they are coherent. The interference between these packets depends on the orientation between the jump vector of the atom and the wave vector (see Fig. 15.9). If a single-crystal specimen is used, in certain crystal directions the linewidth is small and in other directions it is larger.

To exploit Eq. (15.25) a diffusion model is necessary to calculate $\sigma(\boldsymbol{Q}, \omega)$. For random jumps on a Bravais lattice (Markov process) the shape of the

resulting Mössbauer spectrum is a Lorentzian [25, 26]

$$\sigma(\boldsymbol{Q},\omega) \;\propto\; f_{DW}\,\frac{\Delta\Gamma(\boldsymbol{Q})/2}{[\Delta\Gamma(\boldsymbol{Q})/2]^2+(\hbar\omega)^2}\,, \tag{15.26}$$

where $\Delta\Gamma(\boldsymbol{Q})$ is the full peak-width at half maximum. This diffusional broadening depends on the relative orientation between radiation and crystal:

$$\Delta\Gamma(\boldsymbol{Q}) = \frac{2\hbar}{\bar{\tau}}\left(1-\sum_j W_j E_j\right) \quad \text{where} \quad E_j = \frac{1}{N_j}\sum_{k=1}^{N_j}\exp(i\boldsymbol{Q}\cdot\boldsymbol{r}_k)\,. \tag{15.27}$$

W_j is the probability for a displacement to coordination shell j, E_j the corresponding structure factor, N_j denotes the number of sites in the coordination shell j, and $\boldsymbol{r}_k$ are the displacement vectors to sites in shell j.

For diffusion mediated by vacancies, successive jumps of an atom are correlated. An extension of Eq. (15.27) for correlated diffusion has been developed by Wolf [20] on the basis of the so-called encounter model (see Chap. 7). The mean time between encounters is

$$\tau_{enc} = \bar{\tau} Z_{enc}\,, \tag{15.28}$$

where Z_{enc} is the average number of jumps performed by a Mössbauer atom in one encounter. Each complete encounter is treated as an effective displacement not correlated to the previous or following encounter. Wolf showed that the line broadening can be expressed as

$$\Delta\Gamma(\boldsymbol{Q}) = \frac{2\hbar}{\bar{\tau} Z_{enc}}\left(1-\sum_j W_j^{enc} E_j\right)\,, \tag{15.29}$$

where W_j^{enc} is the probability for a displacement of $\boldsymbol{r}_j$ by an encounter with a defect. For further details and for an extension to non-Bravais lattices the reader is referred to [25, 29].

An important consequence of Eq. (15.26) and of Eq. (15.29) is that both $\sigma(\boldsymbol{Q},\omega)$ and $\Delta\Gamma$ depend on the relative orientation between $\boldsymbol{Q}$ and the jump vector $\boldsymbol{r}$ and hence on the orientation of the crystal lattice. This can be exploited by measurements on monocrystals. By varying the crystal orientation, information about the length and direction of the jump vector is obtained. In that respect MBS and QENS are analogous. Examples for the deduction of elementary diffusion jumps will be given in the next section.

15.4 Quasielastic Neutron Scattering (QENS)

The scattering of beams of slow neutrons obtained from nuclear reactors or other high-intensity neutron sources can be used to study structural and dynamic properties of condensed matter. Why neutron scattering is a tool with

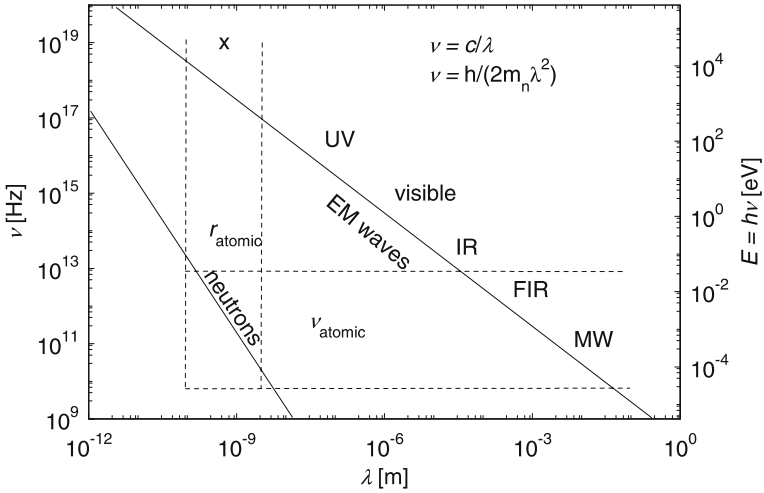

Fig. 15.12. Comparison between the dispersion relations of electromagnetic waves (EM waves) and neutrons

unique properties can be seen from Fig. 15.12, which shows a comparison of the dispersion relations of electromagnetic waves (EM waves) and neutrons. For EM waves the frequency ν and the wavelength λ are related via $\nu = c/\lambda$, where c is the velocity of light. For (non-relativistic) neutrons of mass m_n the dispersion relation is $\nu = h/(2m_n\lambda^2)$. Typical atomic vibration frequencies in a solid, ν_{atomic}, match with far infrared and microwave frequencies of EM waves. On the other hand, typical interatomic distances, r_{atomic}, match with wavelengths of X-rays. Slow and thermal neutrons have the unique feature that their wavelengths and frequencies match atomic frequencies and interatomic distances simultaneously.

Neutrons are uncharged probes and interact with nuclei. In contrast to photons, neutrons have only a weak interaction with matter. This means that neutron probes permit easy access to bulk properties. Since neutrons can penetrate suitable sample containers easily. One can also use sophisticated sample environments, such as wide temperature ranges and high magnetic fields.

The scattering cross section for neutrons is determined by the sample nuclei. The distribution of scattering cross sections in the periodic table is somehow irregular. For example, protons have very high scattering cross sections and are mainly incoherent scatterers. For deuterons the coherent cross section is larger than the incoherent scattering cross section. Carbon, nitrogen, and oxygen have very small incoherent scattering cross sections and are mainly coherent scatterers. For sodium, coherent and incoherent scattering cross sections are similar in magnitude.

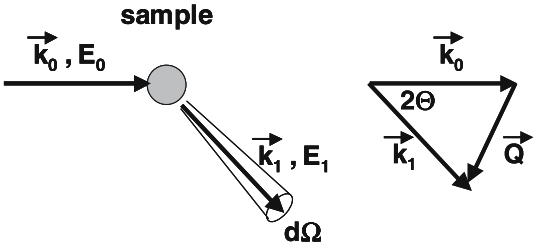

Fig. 15.13. Neutron scattering geometry: in real space (*left*); in momentum space (*right*)

Neutron scattering leads to a spectrum of energy and momentum transfers (Fig. 15.13). The energy transfer is

$$\hbar\omega = E_1 - E_0\,, \tag{15.30}$$

where E_1 and E_0 denote the neutron energies after and before the scattering process, respectively. The corresponding momentum transfer is $\hbar\boldsymbol{Q}$. The scattering vector is

$$\boldsymbol{Q} = \boldsymbol{k}_1 - \boldsymbol{k}_0\,, \tag{15.31}$$

where $\boldsymbol{k}_0$ and $\boldsymbol{k}_1$ are the neutron wave vectors before and after the scattering event. The corresponding neutron wavelenghts are $\lambda_1 = 2\pi/k_1$ and $\lambda_0 = 2\pi/k_0$. The values of

$$Q = \frac{4\pi}{\lambda_0}\sin(\Theta/2) \tag{15.32}$$

(Θ = scattering angle Q = modulus of the scattering vector) vary typically between 1 and 50 nm^{-1}. Therefore, $1/Q$ can match interatomic distances. The scattered intensity in such an experiment is proportional to the so-called scattering function or dynamic structure factor, $S(\boldsymbol{Q},\omega)$, which can be calculated for diffusion processes (see below).

A schematic energy spectrum for neutron scattering with elastic, quasielastic, and inelastic contributions is illustrated in Fig. 15.14. Inelastic peaks are observed, due to the absorption and emission of phonons.

Quasielastic Scattering: Quasielastic scattering must be distinguished from the study of periodic modes such as phonons or magnons by inelastic scattering, which usually occurs at higher energy transfers.

For samples with suitable scattering cross sections, diffusion of atoms in solids can be studied by quasielastic neutron scattering (QENS), if a high-resolution neutron spectrometer is used. QENS, like MBS, is a technique which has considerable potential for elucidating diffusion steps on a microscopic level. Both techniques are applicable to relatively fast diffusion processes only (see Fig. 13.1). QENS explores the diffusive motion in space for a range comparable to the neutron wavelength. Typical jump distances and

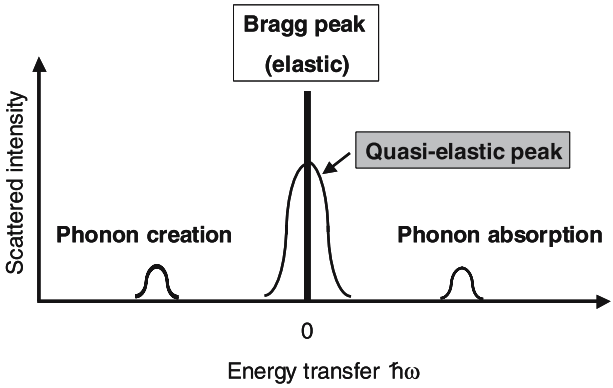

Fig. 15.14. Energy spectrum of neutron scattering (schematic)

diffusion paths between 10^{-8} and 10^{-10} m can be studied. Let us briefly anticipate major virtues of QENS. The full peak-width at half maximum of a Lorentzian shaped quasielastic line is given for small values of Q by

$$\Delta\Gamma = 2DQ^2\,, \tag{15.33}$$

where D is the self-diffusion coefficient [31, 32]. Quasielastic line broadening is due to the diffusive motion of atoms. The pertinent energy transfers $\hbar\omega$ typically range from 10^{-3} to 10^{-7} eV. For larger scattering vectors, $\Delta\Gamma$ is periodic in reciprocal space and hence depends on the atomic jump vector like in MBS. For a particle at rest, we have $\Delta\Gamma = 0$ and a sharp line at $\hbar\omega = 0$ is observed. This elastic line (Bragg peak) results from a scattering process in which the neutron transmits the momentum $\hbar\boldsymbol{Q}$ to the sample as a whole, without energy transfer. For resonance absorption of $\gamma-$rays this corresponds to the well-known Mössbauer line (see above). We have already seen that in MBS a diffusing particle produces a line broadening. QENS is described by similar theoretical concepts as used in MBS [25, 30–32].

Figure 15.15 shows an example of a quasielastic neutron spectrum measured on a monocrystal of sodium according to Göltz et al. [33]. The number of scattered neutrons N is plotted as a function of the energy transfer $\hbar\omega$ for a fixed scattering vector with $Q = 1.3\times10^{-10}$ m^{-1}. The dashed line represents the resolution function of the neutron spectrometer. The observed line is broadened due to the diffusive motion of Na atoms. The quasielastic linewidth depends on the orientation of the momentum transfer and hence of the crystallographic orientation of the crystal (see below).

The Dynamic Structure Factor (Scattering Functions): Let us now recall some theoretical aspects of QENS. The quantity measured in neutron scattering experiments is the intensity of neutrons, ΔI_s, scattered from a collimated mono-energetic neutron beam with a current density I_0. The intensity

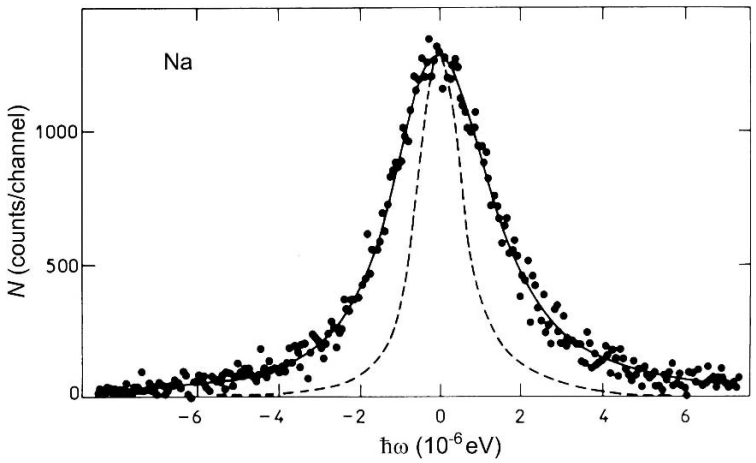

Fig. 15.15. QENS spectrum of a Na monocrystal at 367.5 K according to GÖLTZ ET AL. [33]. *Dashed line*: resolution functionof the neutron spectrometer

of neutrons scattered into a solid angle element, $\Delta\Omega$, and an interval, $\Delta\omega$, from a sample with volume V and number density of scattering atoms, N, (see Fig. 15.13) is given by [31]

$$\Delta I_s = I_0 N V \left(\frac{d^2\sigma}{d\Omega d\omega}\right) \Delta\Omega\Delta\omega\,, \tag{15.34}$$

where the double differential scattering cross section is

$$\frac{d^2\sigma}{d\Omega d\omega} = \frac{k_1}{k_0}\frac{\sigma}{4\pi} S(\boldsymbol{Q},\omega)\,. \tag{15.35}$$

The cross section is factorised into three components: the ratio of the wave numbers k_1/k_0; the cross section for a rigidly bound nucleus, $\sigma = 4\pi b^2$, where b is the corresponding scattering length of the nucleus; the scattering intensity is proportional to the *dynamical structure factor* $S(\boldsymbol{Q},\omega)$. The dynamical structure factor depends on the scattering vector and on the energy transfer defined in Eqs. (15.30) and (15.31). It describes structural and dynamical properties of the sample which do not depend on the interaction between neutron and nuclei.

The interaction of a neutron with a scattering nucleus depends on the chemical species, the isotope, and its nuclear spin. In a mono-isotopic sample, all nuclei have the same scattering length. Then, only coherent scattering will be observed. In general, however, several isotopes are present according to their natural abundance. Each isotope i is characterised by its scattering length b_i. The presence of different isotopes distributed randomly in the sample means that the total scattering cross section is made up of two parts, called *coherent* and *incoherent*.

The theory of neutron scattering is well developed and can be found, e.g., in reviews by Zabel [30], Springer [31, 32] and in textbooks of Squires [37], Lovesey [38], Bee [36], and Hempelmann [39]. Theory shows that the differential scattering cross section can be written as the sum of a coherent and an incoherent part

$$\frac{d^2\sigma}{d\Omega d\omega} = \left(\frac{d^2\sigma}{d\Omega d\omega}\right)_{coh} + \left(\frac{d^2\sigma}{d\Omega d\omega}\right)_{inc} = \frac{k_1}{k_0}\left[\frac{\sigma_{coh}}{4\pi} S_{coh}(\boldsymbol{Q},\omega) + \frac{\sigma_{inc}}{4\pi} S_{inc}(\boldsymbol{Q},\omega)\right] . \tag{15.36}$$

Coherent (index: *coh*) and incoherent (index: *inc*) contributions depend on the composition and the scattering cross sections of the nuclei in the sample. The *coherent scattering* cross section σ_{coh} is due to the average scattering from different isotopes

$$\sigma_{coh} = 4\pi\bar{b}^2 \quad \text{with} \quad \bar{b} = \Sigma c_i b_i \, . \tag{15.37}$$

The *incoherent scattering* is proportional to the deviations of the individual scattering lengths from the mean value

$$\sigma_{inc} = 4\pi\left(\bar{b^2} - \bar{b}^2\right) \quad \text{with} \quad \bar{b^2} = \Sigma c_i b_i^2 \, . \tag{15.38}$$

The bars indicate ensemble averages over the various isotopes present and their possible spin states. The c_i are the fractions of nuclei i.

Coherent scattering is due to interference of partial neutron waves originating at the positions of different nuclei. The coherent scattering function, $S_{coh}(\boldsymbol{Q},\omega)$, is proportional to the Fourier transform of the correlation function of any nuclei. Coherent scattering leads to interference effects and collective properties can be studied. Among other things, this term gives rise to Bragg diffraction peaks.

Incoherent scattering monitors the fate of individual nuclei and interference effects are absent. The incoherent scattering function, $S_{inc}(\boldsymbol{Q},\omega)$, is proportional to the Fourier transform of the correlation function of individual nuclei. Only a mono-isotopic ensemble of atoms with spin $I = 0$ would scatter neutrons in a totally coherent manner. Incoherent scattering is connected to isotopic disorder and to nuclear spin disorder.

We emphasise that it is the theory of neutron scattering that leads to the separation into coherent and incoherent terms. The direct experimental determination of two separate functions, $S_{coh}(\boldsymbol{Q},\omega)$ and $S_{inc}(\boldsymbol{Q},\omega)$, is usually not straightforward, unless samples with different isotopic composition are available. However, sometimes the two contributions can be separated without the luxury of major changes in the isotopic composition. The coherent and incoherent length b_i of nuclei are known and can be found in tables [40]. For example, the incoherent cross section of hydrogen is 40 times larger than the coherent cross section. Then, coherent scattering can be disregarded.

Incoherent Scattering and Diffusional Broadening of QENS Signals: Incoherent quasielastic neutron scattering is particularly useful for diffusion studies. The incoherent scattering function can be calculated for a given diffusion mechanism. Let us first consider the influence of diffusion on the scattered neutron wave in a simplified, semi-classical way: in an ensemble of incoherent scatterers, only the waves scattered by the same nucleus can interfere. At low temperatures the atoms stay on their sites during the scattering process; this contributes to the elastic peak. The width of the elastic peak is then determined by the energy resolution of the neutron spectrometer. At high temperatures the atoms are in motion. Then the wave packets emitted by diffusing atoms are 'cut' to several shorter 'packets', which leads to diffusional broadening of the elastic line. This is denoted as incoherent quasielastic scattering. Like in MBS the interference between wave packets emitted by the same nucleus depends on the relative orientation between the jump vector of the atom and the scattering direction. Therefore, in certain crystal direction the linewidth will be small while in other directions it will be large.

For a quantitative description of the incoherent scattering function the van Hove self-correlation function $G_s(\boldsymbol{r}, t)$ is used as a measure of diffusive motion. The incoherent scattering function is proportional to the Fourier transform of the self-correlation function

$$S_{inc}(\boldsymbol{Q}, \omega) = \frac{1}{2\pi} \int \int G_s(\boldsymbol{r}, t) \exp\left[i(\boldsymbol{Q}\boldsymbol{r} - \omega t)\right] \mathrm{d}\boldsymbol{r} \mathrm{d}t \,. \tag{15.39}$$

When atomic motion can simply be described by continuous translational diffusion in three dimensions, the self-correlation function $G_s(\boldsymbol{r}, t)$ takes the form of a Gaussian (see Chap. 3)

$$G_s(\boldsymbol{r}, t) = \frac{1}{(4\pi D t)^{3/2}} \exp\left(-\frac{r^2}{4Dt}\right) , \tag{15.40}$$

with D denoting the self-diffusion coefficient of atoms. Its Fourier transform in space

$$S(\boldsymbol{Q}, t) = \exp\left(-Q^2 D t\right) \tag{15.41}$$

is an exponential function of time, the time Fourier transform of which is a Lorentzian:

$$S_{inc}(\boldsymbol{Q}, \omega) \; = \frac{1}{\pi} \, \frac{DQ^2}{(DQ^2)^2 + \omega^2} \,. \tag{15.42}$$

This equation shows that for small Q values the linewidth of the quasielastic line is indeed given by Eq. (15.33). It is thus possible to determine the diffusion coefficient from a measurement of the linewidth as a function of small scattering vectors.

In the derivation of Eq. (15.42) the continuum theory of diffusion was used for the self-correlation function. This assumption is only valid for small scattering vectors $|Q| << 1/d$, where d is the length of the jump vectors in the

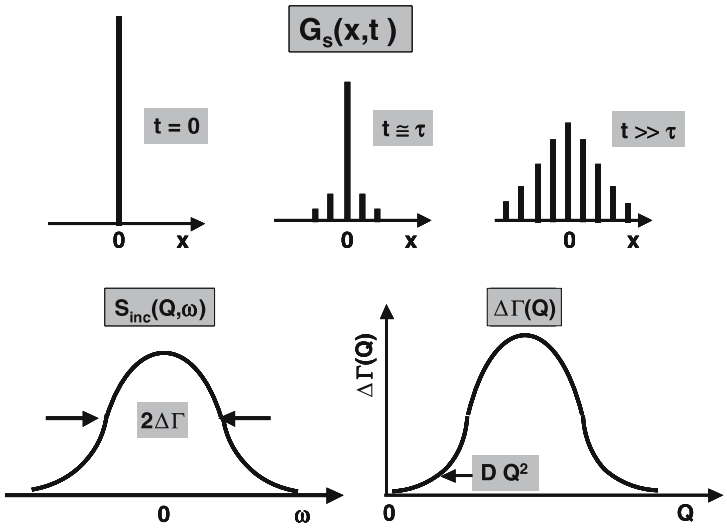

Fig. 15.16. *Top*: Self-correlation function G_s for a one-dimensional lattice. *Top*: The height of the *solid lines* represents the probability of occupancy per site. Asymptotically, the envelope approaches a Gaussian. *Bottom*: Incoherent contribution $S_{inc}(Q,\omega)$ to the dynamical structure factor and quasi-elastic linewidth $\Delta\Gamma$ *versus* scattering vector Q. According to [32]

lattice. For jump diffusion of atoms on a Bravais lattice the self-correlation function G_s can be obtained according to Chudley and Elliot [41]. The probability $P(\boldsymbol{r}_n, t)$ to find a diffusing atom on a site $\boldsymbol{r}_n$ at time t is calculated using the *master equation* for $P(\boldsymbol{r}_n, t)$:

$$\frac{\partial P(\boldsymbol{r}_n, t)}{\partial t} = -\frac{1}{\bar{\tau}} P(\boldsymbol{r}_n, t) + \frac{1}{Z\bar{\tau}} \sum_{i=1}^{Z} P(\boldsymbol{r}_n + \boldsymbol{l}_i, t)\,. \tag{15.43}$$

$\boldsymbol{l}_i$ (i =1, 2, ... Z) is a set of jump vectors connecting a certain site with its Z neighbours. $\bar{\tau}$ denotes the mean residence time. The two terms in Eq. (15.43) correspond to loss and gain rates due to jumps to and from adjacent sites respectively. With the initial condition $P(\boldsymbol{r}_n, 0) = \delta(\boldsymbol{r}_n)$, the probability $P(\boldsymbol{r}, t)$ becomes equivalent to the self-correlation function $G_s(\boldsymbol{r}_n, t)$. A detailed theory of the master equation can be found in [42, 43]. If $P(\boldsymbol{r}_n, t)$ is known the incoherent scattering function is obtained by Fourier transformation in space and time according to Eq. (15.39). For a one-dimensional lattice G_s is illustrated in Fig. 15.16.

The classical model for random jump diffusion on Bravais lattices via nearest-neighbour jumps was derived by Chudley and Elliot in 1961 [35] (see also [36]). The incoherent scattering function for random jump motion on a Bravais lattice is given by

$$S_{inc}(\boldsymbol{Q},\omega) = \frac{2}{\pi}\,\frac{\Delta\Gamma(\boldsymbol{Q})}{\Delta\Gamma(\boldsymbol{Q})^2+\omega^2}\,. \tag{15.44}$$

The function $\Delta\Gamma(\boldsymbol{Q})$ is determined by the lattice structure, the jumps which are possible, and the jump rate with which they occur. For the scattering of neutrons in a particular direction $\boldsymbol{Q}$, the variation with change in energy $\hbar\omega$ is Lorentzian in shape with a linewidth given by $\Delta\Gamma$.

In the case of polycrystalline samples, the scattering depends on the modulus $Q = |\boldsymbol{Q}|$ only, but still consists of a single Lorentian line with linewidth

$$\Delta\Gamma = \frac{2}{\bar{\tau}}\left[1 - \frac{\sin(Qd)}{Qd}\right]. \tag{15.45}$$

Here $\bar{\tau}$ is the mean residence time for an atom on a lattice site and d the length of the jump vector.

For a monocrystal with a simple cubic Bravais lattice one gets for the orientation dependent linewidth

$$\Delta\Gamma(\boldsymbol{Q}) = \frac{2}{3\bar{\tau}}\left[3 - \cos(Q_x d) - \cos(Q_y d) - \cos(Q_z d)\right], \tag{15.46}$$

where Q_x, Q_y, Q_z are the components of $\boldsymbol{Q}$ and d is the length of the jump vector. The linewidth is a periodic function in reciprocal space. It has a maximum at the boundary of the Brillouin zone and it is zero if a reciprocal lattice point $\boldsymbol{G}$ is reached. This line narrowing is a remarkable consequence of quantum mechanics.

For vacancy-mediated diffusion successive jumps of atoms are correlated. Like in the case of MBS, the so-called encounter model can be used for low vacancy concentrations (see Chap. 7). A vacancy can initiate several correlated jumps of the same atom, such that one encounter comprises Z_{enc} atomic jumps. As we have seen in Chap. 7, the time intervals between subsequent atomic jumps within the same encounter are very short as compared to the time between encounters. As a consequence, the quasielastic spectrum can be calculated within the framework of the Chudley and Elliot model, where the rapid jumps within the encounters are treated as instantaneous. The linewidth of the quasielastic spectrum is described by [33]

$$\Delta\Gamma = \frac{2}{\bar{\tau} Z_{enc}}\left[1 - \sum_{\boldsymbol{r}_m} W_{enc}(\boldsymbol{r}_m)\cos(\boldsymbol{Q}\boldsymbol{r}_m)\right], \tag{15.47}$$

where $W_{enc}(\boldsymbol{r}_m)$ denotes the probability that, during an encounter, an atom originally at $\boldsymbol{r}_m = 0$ has been displaced to lattice site $\boldsymbol{r}_m$ by one or several jumps. The probabilities can be obtained, e.g., by computer simulations. A detailed treatment based on the encounter model can be found in a paper by Wolf [46]. Equation (15.47) is equivalent to Eq. (15.29) already discussed in the section about Mössbauer spectroscopy.

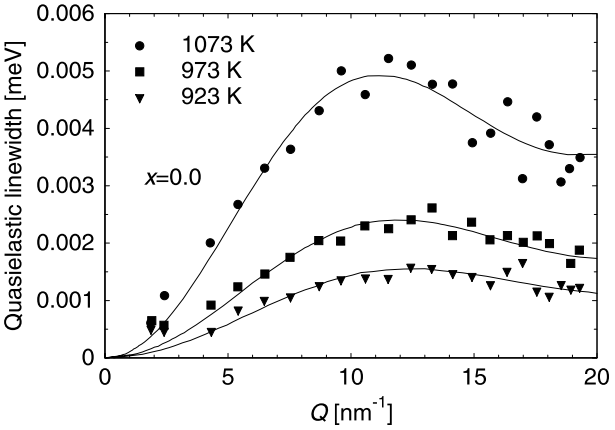

Fig. 15.17. Quasielastic linewidth as a function of the modulus $Q = |\boldsymbol{Q}|$ for polycrystalline Na_2PO_4 according to Wilmer and Combet [47]. *Solid lines*: fits of the Chudley-Elliot model

15.4.1 Examples of QENS studies

Let us now consider examples of QENS studies, which illustrate the potential of the technique for polycrystalline material and for monocrystals.

Na self-diffusion in ion-conducting rotor phases: Sodium diffusion in solid solutions of sodium orthophosphate and sodium sulfate, xNa_2SO_4 $(1\text{-}x)Na_3PO_4$, has been studied by Wilmer and Combet [47]. These materials belong to a group of high-temperature modifications with both fast cation conductivity and anion rotational disorder and are thus termed as fast ion-conducting rotor phases. The quasielastic linewidth of polycrystalline samples has been measured as a function of the momentum transfer. In the case of polycrystalline samples, the scattering depends on the modulus of $Q = |\boldsymbol{Q}|$ only, but still consist of a single Lorentzian line with linewidth Eq. (15.45). The Q-dependent linebroadening is shown for Na_2PO_4 at various temperatures in Fig. 15.17. The linewidth parameters $\bar{\tau}$ and d have been deduced. Obviously, the jump rates $\bar{\tau}^{-1}$ incresase with increasing temperature. Much more interesting is that the jump distance could be determined. It turned out that sodium diffusion is dominated by jumps between neighbouring tetrahedrally coordinated sites on an fcc lattice, the jump distance being half of the lattice constant.

At very low values of Q, quasielastic broadening does no longer depend on details of the jump geometry since the linewidth is dominated by the long-range diffusion via Eq. (15.33). The linebroadening at the two lowest accessible Q values (1.9 and $2.9\,\mathrm{nm}^{-1}$) was used to determine the sodium self-diffusivites [47]. An Arrhenius plot of the sodium diffusivities is shown in

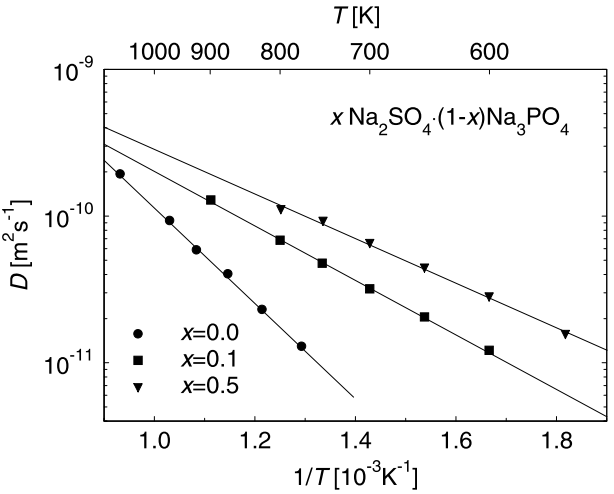

Fig. 15.18. Self-diffusion of Na in three $xNa_2SO_4(1\text{-}x)Na_3PO_4$ rotor phases according to Wilmer and Combet [47]

Fig. 15.18. The activation enthalpies decrease from 0.64 eV for pure Na_3PO_4 to 0.3 eV for a sulphate content of 50%:

Na self-diffusion in Na single-crystals: Quasielastic scattering of sodium single crystals has been investigated by Göltz et al. [33] and Ait-Salem et al. [34] and analysed in terms of Eq. (15.47). It was demonstrated that self-diffusion of sodium occurs by nearest-neighbour jumps in the bcc lattice. Figure 15.19 shows the linebroadening as a function of the momentrum transfer $\boldsymbol{Q}$ in directions parallel to $\langle 111\rangle$, $\langle 110\rangle$, and $\langle 100\rangle$ at 362.2 K. Model calculations are also shown, assuming a monovacancy mechnaism with nearest-neighbour jumps on with a $\langle 111\rangle$ jumps. The results show that diffusion proceeds via nearest-neighbour jumps.

H diffusion in palladium: QENS measurements have been widely used to study diffusion of H-atoms in interstitial solutions of hydrogen in palladium. Interstitial diffusion is uncorrelated (see Chap. 7). It was shown, for example, that H-atoms jump between nearest-neighbour octahedral sites of the interstitial lattice of fcc Pd [44, 45].

15.4.2 Advantages and Limitations of MBS and QENS

For MBS diffusion studies it is necessary to heat the sample to sufficiently high temperatures that the mean residence time of an atom on a lattice site, $\bar{\tau}$, is comparable to or less than the half-life of the Mössbauer level τ_N. For metals, this implies temperatures not much below the melting temperature.

Mössbauer spectroscopy is sensitive to the elementary steps of diffusion on a microscopic scale. A direct determination of *jump vectors* and *jump rates*

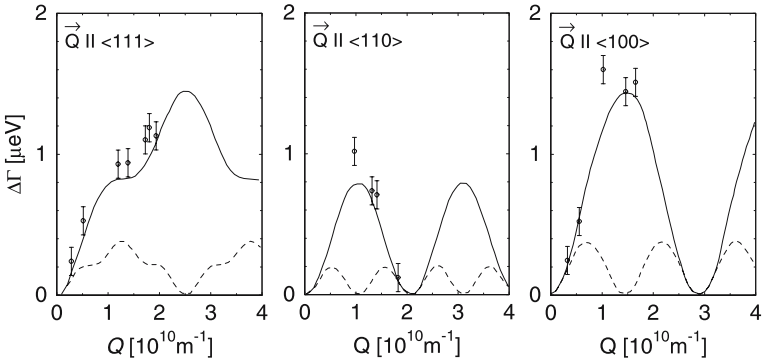

Fig. 15.19. Self-diffusion of Na metal. Dependence of the QENS line broadening in three major crystallographic directions. Theoretical curves have been calculated for a monovacancy mechanism assuming nearest-neighbour junps (*solid lines*) and $a\langle 111\rangle$ jumps (*dotted line*). From VOGL AND PETRY [27] according to [33, 34]

is possible, when single-crystal samples are used and the line-broadening is measured as a function of crystal orientation. In addition, one can deduce the diffusion coefficient and compare it with data obtained, e.g., by tracer diffusion studies. However, this is not the main virtue of a microscopic method.

The nuclei studied in MBS must have a large value of the recoilless fraction, which limits the number of good isotopes to a few species. As already mentioned the major 'workhorse' of Mössbauer spectroscopy is ^{57}Fe. The isotopes ^{119}Sn, ^{151}Eu, and ^{161}Dy are less favourable but still useful isotopes for diffusion studies. Mössbauer diffusion studies in practice require a diffusional line-broadening that is comparable or larger than the natural linewidth of the Mössbauer transition. Only relatively large diffusion coefficients can be measured. For example, ^{57}Fe diffusion coefficients in the range 10^{-14} to $10^{-10}\,\mathrm{m^2\,s^{-1}}$ are accessible.

For diffusion studies by quasielastic neutron scattering (QENS) it is necessary to keep the sample at temperatures where the mean residence time of atoms on a lattice site, $\bar{\tau}$, is short enough to produce a diffusional broadening, which exceeds the energy resolution of the neutron spectrometer. For time-of-flight spectrometry the resolution is in the range of μeV to 0.1 meV. This allows a range of diffusion coefficients between about 10^{-12} and $10^{-8}\,\mathrm{m^2\,s^{-1}}$ to be covered. Diffusion coefficients can be determined directly from the Q^2 dependence of the linewidth.

QENS has mainly been used to study hydrogen and sodium diffusion in solids. A prerequisite of QENS is that the element of interest has a large enough incoherent scattering cross section as compared to the coherent scattering cross section. Only few elements such as hydrogen, sodium, and vanadium fulfill this condition. In these cases QENS is unique, since there are no Mössbauer isotopes for these elements. Otherwise, in luxury experiments dif-

ferent mixtures of isotopes can be used to separate coherent and incoherent contributions to scattering. The major merits of QENS and MBS are that both permit the investigation of the elementary steps of diffusion in solids on a scale of atomic dimensions and times. Both techniques are applicable to fast diffusion processes (see Fig. 13.1).

References

1. N. Bloembergen, E.M. Purcell, R.V. Pound, Phys. Rev. **73**, 679 (1948)
2. A. Abragam, *The Priciples of Nuclear Magnetism*, University Press, Oxford, 1973
3. C.P. Slichter, *Principles of Magnetic Resonance*, Springer-Verlag, Berlin, 1989
4. M. Mehring, *High Resolution NMR Spectroscopy in Solids*, Springer-Verlag, Berlin, 1983
5. H.T. Stokes, *Study of Diffusion in Solids by Pulsed Nuclear Magnetic Resonance*, in: *Nontraditional Methods in Diffusion*, G.E. Murch, H.K. Birnbaum, J.R. Cost (Eds.), The Metallurgical Society of AIME, Warrendale, 1984. p. 39
6. A.R. Allnatt, A.B. Lidiard, *Atomic Transport in Solids*, Cambridge University Press, 1993
7. G. Majer, *Die Methoden der Kernspinresonanz zum Studium der Diffusion von Wasserstoff in Metallen und intermetallischen Verbindungen*, Cuvillier Verlag, Göttingen, 2000
8. P. Heitjans, A. Schirmer, S. Indris, *NMR and β-NMR Studies of Diffusion in Interface-Dominated and Disordered Solids*, in: *Diffusion in Condensed Matter – Methods, Materials, Models*, P. Heitjans, J. Kärger (Eds.), Springer-Verlag, 2005
9. P. Heitjans, S. Indris, M. Wilkening, *Solid-State Diffusion and NMR*, in *Diffusion Fundamentals – Leipzig 2005*, J. Kärger, F. Grinberg, P. Heitjans (Eds.), Leipziger Universitätsverlag, 2005
10. B.C. Gerstein, C.R. Dybowski, *Transient Techniques in NMR of Solids*, Academic Press, New York, 1985
11. H.C. Torrey, Phys. Rev. **104**, 563 (1956)
12. E.L. Hahn, Phys. Rev. **80**, 580 (1950)
13. E.O. Stejskal, J.E. Tanner, J. Chem. Phys. **42** 288 (1965)
14. D.W. McCall, D.C. Douglas, E.W. Anderson, Ber. Bunsenges. **67**, 336 (1963)
15. P. Stilbs, in: *Progress in NMR Spectroscopy*, J.W. Emsley, J. Feeney, L.H. Sutcliffe (Eds.), Pergamon Press, Oxford, **19**, 1988
16. J. Kärger, G. Fleischer, U. Roland, in: *Diffusion in Condensed Matter*, J. Kärger, P. Heitjans, R. Haberlandt (Eds.), Vieweg-Verlag, 1998, p. 144
17. A. Feinauer, G. Majer, A. Seeger, Defect and Diffusion Forum **143–147**, 881 (1997)
18. A. Feinauer, G. Majer, Phys. Rev. **B 64**,134302 (2001)
19. H.C. Torrey, Phys. Rev. **96**, 690 (1954)
20. D. Wolf, *Spin Temperature and Nuclear Spin Relaxation in Matter*, Clarendon Press, Oxford, 1979
21. I.R. MacGillivray, C.A. Sholl, J. Phys. C **19**, 4771 (1986); C.A. Sholl, J. Phys. C **21**, 319 (1988)

22. G. Majer, presented at: International Max Planck Research School for Advanced Materials, April 2006
23. R.L. Mössbauer, Z. Physik **151**, 124 (1958)
24. K.S. Singwi, A. Sjölander, Phys. Rev. **120** 1093 (1960)
25. G. Vogl, R. Feldwisch, *The Elementary Diffusion Step in Metals Studied by Methods from Nuclear Solid-State Physics*, in: *Diffusion in Condensed Matter*, J. Kärger, P. Heitjans, R. Haberlandt (Eds.), Vieweg-Verlag, 1998, p. 40
26. G. Vogl, B. Sepiol, *The Elementary Diffusion Step in Metals Studied by the Interference of γ-Rays, X-Rays and Neutrons*, in: *Diffusion in Condensed Matter – Methods, Materials, Models*, P. Heitjans, J. Kärger (Eds.), Springer-Verlag, 2005
27. G. Vogl, W. Petry, *Diffusion in Metals studied by Mössbauer Spectroscopy and Quasielastic Neutron Scattering*, in: Festkörperprobleme XXV (Advances in Solid State Physics), P. Grosse (Ed.), Braunschweig, F. Vieweg und Sohn, 1985, P. 655
28. L. van Hove, Phys. Rev. **95**, 249 (1954)
29. J.G. Mullen, *Mössbauier Diffusion Studies*, in: *Nontraditional Methods in Diffusion*, G.E. Murch, H.K. Birnbaum, J.R. Cost (Eds.), The Metallurgical Society of AIME, Warrendale, 1984, p.59
30. H. Zabel, *Quasi-Elastic Neutron Scattering: a Powerful Tool for Investigating Diffusion in Solids*, in: *Nontraditional Methods in Diffusion*, G.E. Murch, H.K. Birnbaum, J.R. Cost (Eds.), The Metallurgical Society of AIME, Warrendale, 1984. p. 1
31. T. Springer, *Diffusion Studies of Solids by Quasielastic Neutron Scattering*, in: *Diffusion in Condensed Matter*, J. Kärger, P. Heitjans, R. Haberlandt (Eds.), Vieweg-Verlag, 1998., p. 59
32. T. Springer, R.E. Lechner, *Diffusion Studies of Solids by Quasielastic Neutron Scattering*, in: *Diffusion in Condensed Matter – Methods, Materials, Models*, P. Heitjans, J. Kärger (Eds.), Springer-Verlag, 2005
33. G. Göltz, A. Heidemann, H. Mehrer, A. Seeger, D. Wolf, Philos. Mag. **A 41**, 723 (1980)
34. M. Ait-Salem, T. Springer, A. Heidemann, B. Alefeld, Philos. Mag. **A 39**, 797 (1979)
35. C.T. Chudley, R.J. Elliiot. Proc. Phys. Soc. **77**, 353 (1961)
36. M. Bee, *Quasielastic Scattering*, Adam Hilger, Bristol, 1988
37. G.L. Squires, *Introduction to the Theory of Thermal Neutron Scattering*, Cambridge University Press, 1978
38. S.W. Lovesey, *Theory of Neutron Scattering from Condensed Matter*, Clarendon Press, Oxford, 1986
39. R. Hempelmann, *Quasielastic Neutron Scattering and Solid-State Diffusion*, Oxford Science Publication, 2000
40. L. Koester, H. Rauch, E. Seyman, Atomic Data and Nuclear Data Tables **49**, 65 (1991)
41. C.T. Chudley, R.J. Elliot, Proc. Phys. Soc. **77**, 353 (1961) (see [35])
42. K.W. Kehr, K. Mussawisade, Th. Wichmann, *Diffusion of Particles on Lattices*, in: *Diffusion in Condensed Matter*, J. Kärger, P. Heitjans, R. Haberlandt (Eds.), Vieweg-Verlag, 1998, p. 265
43. K.W. Kehr, K. Mussawisade, G. M. Schütz, G. Th. Wichmann, *Diffusion of Particles on Lattices*, in: *Diffusion in Condensed Matter – Methods, Materials, Models*, P. Heitjans, J. Kärger (Eds.), Springer-Verlag, 2005

44. K. Sköld, G. Nelin, J. Phys. Chem. Solids **28**, 2369 (1967)
45. J.M. Rowe, J.J. Rush, L.A. de Graaf, G.A. Ferguson, Phys. Rev. Lett **29**, 1250 (1972)
46. D. Wolf, Appl. Phys. Letters **30**, 617 (1977)
47. D. Wilmer, J. Combet, Chemical Physics **292**, 143 (2003)